Biomaterials 33 (2012) 6998–7007

Contents lists available at SciVerse ScienceDirect

Biomaterials

journal homepage: www.elsevier.com/locate/biomaterials

The osteogenic differentiation of human bone marrow MSCs on HUVEC-derived ECM and β-TCP scaffold

Yunqing Kang [a], Sungwoo Kim [a], Julius Bishop [a], Ali Khademhosseini [b,c,d], Yunzhi Yang [a,*]

[a] Department of Orthopedic Surgery, Stanford University, 300 Pasteur Drive, Edwards R155, Stanford, CA 94305, USA
[b] Center for Biomedical Engineering, Department of Medicine, Brigham and Women's Hospital, Harvard Medical School, Cambridge, MA 02139, USA
[c] Harvard-MIT Division of Health Sciences and Technology, Massachusetts Institute of Technology, Cambridge, MA 02139, USA
[d] Wyss Institute for Biologically Inspired Engineering, Harvard University, Boston, MA 02115, USA

ARTICLE INFO

Article history:
Received 31 May 2012
Accepted 22 June 2012
Available online 15 July 2012

Keywords:
Extracellular matrix
HUVEC
hMSC
Osteogenesis
β-TCP

ABSTRACT

Extracellular matrix (ECM) serves a key role in cell migration, attachment, and cell development. Here we report that ECM derived from human umbilical vein endothelial cells (HUVEC) promoted osteogenic differentiation of human bone marrow mesenchymal stem cells (hMSC). We first produced an HUVEC-derived ECM on a three-dimensional (3D) beta-tricalcium phosphate (β-TCP) scaffold by HUVEC seeding, incubation, and decellularization. The HUVEC-derived ECM was then characterized by SEM, FTIR, XPS, and immunofluorescence staining. The effect of HUVEC-derived ECM-containing β-TCP scaffold on hMSC osteogenic differentiation was subsequently examined. SEM images indicate a dense matrix layer deposited on the surface of struts and pore walls. FTIR and XPS measurements show the presence of new functional groups (amide and hydroxyl groups) and elements (C and N) in the ECM/β-TCP scaffold when compared to the β-TCP scaffold alone. Immunofluorescence images indicate that high levels of fibronectin and collagen IV and low level of laminin were present on the scaffold. ECM-containing β-TCP scaffolds significantly increased alkaline phosphatase (ALP) specific activity and up-regulated expression of osteogenesis-related genes such as *runx2*, *alkaline phosphatase*, *osteopontin* and *osteocalcin* in hMSC, compared to β-TCP scaffolds alone. This increased effect was due to the activation of MAPK/ERK signaling pathway since disruption of this pathway using an ERK inhibitor PD98059 results in down-regulation of these osteogenic genes. Cell-derived ECM-containing calcium phosphate scaffolds is a promising osteogenic-promoting bone void filler in bone tissue regeneration.

1. Introduction

Extracellular matrix (ECM) is a fibrillar basement network of secreted proteins that is composed mainly of collagens and proteoglycans. ECM provides appropriate microenvironment to support cell adhesion and direct cell behaviors such as proliferation, and differentiation [1–3]. *In vivo*, ECM is initially produced by cells and subsequently formed into a three-dimensional (3D) network [3].

In an attempt to engineer similar microenvironments in tissue engineered scaffolds for regenerative medicine applications, previous studies have utilized decellularized ECM derived from human or animal tissues and organs, typically urinary bladder, heart valves or small intestine [4–6], to produce biological scaffolds. However, potential pathogen transmission and the dimensions of the original tissue limit the application of decellularized ECM from human or animal tissue [4,5,7]. In contrast, the use of synthetic scaffolds carries little to no risk of infectious disease transmission and has the added advantage of easy formulation. However, these synthetic scaffolds rarely provide the necessary biological stimulus for appropriate tissue development.

In order to reproduce ECM-like function in synthetic scaffolds, previous studies have utilized ECM proteins such as vitronectin, collagen, laminin and fibronectin to coat the surface of polymers, ceramics, and hydrogels [8–13,14]. Kundu and Putnam demonstrated that vitronectin and collagen I coated onto PLGA polymer film regulated the osteogenic behavior of hMSC through MAPK/ERK signaling pathway [12,13] while Klees et al. reported that laminin-5 stimulated the osteogenic differentiation of hMSC [15]. Although these studies demonstrate that ECM proteins can enhance cell attachment and differentiation, it is difficult to reproduce the exact composition and function of native ECM using protein-coating methods alone [16].

* Corresponding author. Tel.: +1 650 723 0772; fax: +1 650 724 5401.
E-mail address: ypyang@stanford.edu (Y. Yang).

0142-9612/$ – see front matter © 2012 Elsevier Ltd. All rights reserved.
http://dx.doi.org/10.1016/j.biomaterials.2012.06.061

Therefore, creating a native ECM on a synthetic scaffold may facilitate cell development by combining biological cues with three-dimensional (3D) mechanical support. Cell-derived ECM fabricated onto 3D scaffolds has recently garnered increased attention with several studies showing promising results [17–20,21]. Mikos and colleagues showed that titanium fiber meshes containing ECM derived from rat marrow stromal cells increased bone matrix deposition *in vitro* when compared to those directly grown on titanium fiber mesh or polymeric scaffold alone [22–24,25]. Chen and colleagues demonstrated that bone marrow cell-derived ECM facilitates expansion of mesenchymal colony-forming units *in vitro* while maintaining their stem cell properties [26]. These results suggest that cell-derived ECM creates a micro-environment conducive to osteoblastic cell differentiation. Therefore, we hypothesize that HUVEC-derived ECM-containing porous ceramic scaffolds can promote osteogenic differentiation of hMSC.

There were three goals of this study. The first was to investigate the feasibility of depositing HUVEC-derived ECM on the surface of a porous β-TCP bioceramic scaffold. The second was to see if HUVEC-derived ECM would enhance osteogenic differentiation of hMSC, and the third was to assess the function of the MAPK/ERK signaling pathway in the osteogenic process. We first established the protocol of HUVEC-derived ECM on porous β-TCP scaffolds and characterized it using scanning electron microscope (SEM), Fourier transmission infrared spectrum (FTIR), X-ray photoelectron spectroscopy (XPS), and immunofluorescence staining. Then osteogenic differentiation of hMSC was investigated through evaluation of alkaline phosphatase (ALP) specific activity and gene expression of osteogenic genes, including alkaline phosphatase (*alp*), runt-related transcription factor 2 (*runx2*), osteopontin (*opn*) and osteocalcin (*oc*). Finally, an osteogenic signaling pathway MAPK/ERK was also studied.

2. Materials and methods

2.1. Materials

β-TCP powder (specific surface area: 17 m^2/g) was obtained from Nanocerox, Inc. (Ann Arbor, Michigan). Paraffin granules purchased from Fisher Scientific (Pittsburgh, USA) were used to fabricate small beads as porogen.

An MSCGM™ BulletKit™, EBM™ (endothelial basal medium), and an EGM™ (endothelial growth media) SingleQuots™ Kit were purchased from Lonza, Inc. Anti-human laminin monoclonal antibody (MAB1921) was obtained from Millipore (Billerica, MA). Mouse anti-human monoclonal antibodies to collagen IV (ab6311) and to fibronectin (ab26245) were purchased from Abcam. Mouse monoclonal osteocalcin antibody (sc73464) was purchased from Santa Cruz Biotechnology (Santa Cruz, CA). Rabbit anti-human polyclonal antibody ERK1/2 and phospho-ERK1/2 (Thr202/Tyr204), and the secondary antibody Alexa Fluor® 594 (goat anti-mouse, 2 mg/mL) were purchased from Invitrogen (Carlsbad, CA). Anti-rabbit IgG (H + L) HRP conjugate was purchased from Promega. MEK1/2 inhibitor PD98059 was purchased from Sigma–Aldrich.

2.2. Preparation of β-TCP scaffolds

The process to fabricate β-TCP scaffolds using a template-casting method was described in previous studies [27,28]. In short, β-TCP powder, dispersant (Darvan® C), surfactant (Surfonal®), and carboxymethyl cellulose powder were mixed in distilled water to form slurry. Paraffin beads with designed size were packed into a customized mold and heated to partially melt the beads and form the template. The β-TCP ceramic slurry was then cast onto the template. The slurry can thoroughly fill the template under vacuum environment. The as-cast template was solidified for two days and then dehydrated in a series of graded ethanol solutions. After the dehydration, the dehydrated ceramic green body was put in an alumina dish and sintered at 1250 °C for 3 h. The morphology of β-TCP scaffolds was characterized by scanning electron microscopy. The diameter of the scaffolds used for this study was 7–8 mm and the height was 5–6 mm. The porosity of the scaffolds was 82.5 ± 0.1% and the pore size ranged from 350 μm to 500 μm [29].

2.3. Cell culture

HUVEC was provided from the laboratory of the late Dr. J. Folkman (Children's Hospital, Boston). hMSC was provided by Dr. Melero-Martin from Children's Hospital, Boston. The hMSC can differentiate into adipogenic, chondrogenic, and osteogenic lineages [30]. The hMSC were cultured in MSCBM, which is a non-differentiating growth medium containing 10% fetal bovine serum (FBS) and 1× glutamine–penicillin–streptomycin (GPS; Invitrogen). HUVEC were cultured in EBM-2 containing supplements from EGM-2 kit and 10% FBS. The cell medium was changed every 3 days. Cells below passage 9 were used in all the experiments.

2.4. Production of ECM on β-TCP scaffolds

HUVEC were cultured in EBM-2 and trypsinized after confluence. 1×10^5 cells suspended in 100 μl medium were seeded onto scaffolds and then incubated for 1 h for cell attachment on the surface of scaffolds; afterwards, additional culture medium was added to culture cells on the scaffold for 14 days. Medium was changed every 3 days. At the designed time points, cell/scaffolds were washed in PBS and then HUVEC were stripped off from the scaffolds in a mixture solution of 0.5% Triton X-100 and 20 mM NH_4OH for 5 min according to previously reported methods [31,32], leaving structurally-intact ECM exposed and uniformly attached on the surface of inner walls of scaffolds. Finally, ECM-deposited scaffold surfaces were gently washed 5 times using PBS and air-dried in the biological hood for further use.

2.5. Identification and characterization of ECM deposited on β-TCP scaffolds

2.5.1. Scanning electron microscope (SEM)

The surface morphology of β-TCP scaffold and ECM/β-TCP scaffold were examined using an SEM (FEI, USA). The scaffolds were sputter-coated with gold before imaging. The operated voltage was set at a 15 kV.

2.5.2. Immunofluorescent staining of matrix

To study the protein components and distribution pattern of HUVEC-derived ECM on β-TCP scaffolds, immunofluorescent staining was performed. Three proteins, collagen IV, fibronectin and laminin as biomarkers of ECM components, were immunofluorescent stained. After decellularization, ECM/β-TCP scaffolds were washed three times in PBS. A 5% BSA–PBS buffer solution was used to block the samples for 1 h at room temperature, and then primary antibodies, including mouse anti-human collagen IV (dilution 1:200), fibronectin (dilution 1:100), and laminin (dilution 1:100) in 1% BSA–PBS, were added into the sample followed by incubation overnight at 4 °C. After washing with PBS, a secondary antibody (Alexa Fluor® 594, 2 μg/ml, Invitrogen) in 1% BSA–PBS was added into the samples and incubated in the dark for 1 h at room temperature. Finally, the cell nuclei were counterstained with DAPI (5 μg/ml) for 1 min and then extensively washed with PBS. The fluorescent staining was imaged by confocal microscopy (CSLM, Olympus IX81).

2.5.3. Fourier transmission infrared spectrum (FTIR)

FTIR analysis was carried out to determine components of ECM/β-TCP using an attenuated total reflection system on a Nicolet spectrometer. FTIR spectra were recorded with 100 scans at 4.0 cm^{-1} resolution. Spectra were normalized to a background spectrum. A dry system was used to prevent atmospheric moisture.

2.5.4. X-ray photoelectron spectroscopy (XPS)

XPS was conducted to investigate the surface elements of ECM on β-TCP (detectable depth 3–5 nm). A focused monochromatic Al-Kα X-ray (1486.6 eV) was used as excitation source. To bombard the sample, X-rays were set to 40 W of power, a running voltage of 15 kV and a sampling area of 200 μm in diameter. The binding energy (1100–0 eV) was recorded in survey scan spectra at 0.5 eV steps, and the pass energy was set at 140 eV. Elemental spectra of C1s, O1s, N1s, Ca2s, P2p were scanned at a high resolution with 0.1 eV intervals. The percentages of each major element were automatically calculated by equipment-associated Multipak software. Binding energies of elemental spectra were autoshift-scaled to the spectra of C1s peak which was set at 284.7 eV. A control sample consisting of decellularized ECM collected from culture plates was also measured.

2.6. Proliferation and osteogenic differentiation assays

hMSC were seeded at a density of 1×10^5 cells/scaffold on ECM/β-TCP and β-TCP scaffolds in MSCBM non-differentiation medium, and then the culture medium was changed to hMSC osteogenic media, which contains 10% FBS, 10 mM β-glycerophosphate, 10 nM dexamethasone, and 50 μg/ml ascorbic acid. For the experimental groups involving the inhibitor PD98059, fresh osteogenic media containing inhibitor PD98059 at a final concentration of 50 μM were added. On each media change, fresh inhibitor was added into the fresh media. At each time point, cells were harvested from scaffolds. After rinsing the samples in PBS, the samples were frozen at −20 °C.

Concentration of double-stranded DNA (dsDNA), which represents cell proliferation, was quantified in a fluorometric assay. At the determined time point, Cells were lysed in a 0.2% Triton X-100 solution followed by three freeze/thaw cycles. During each cycle, cells/scaffolds were frozen to −80 °C for 20 min followed by thawing to 37 °C for another 20 min. To homogenize cell lysates solution, samples were finally sonicated on ice for 1 min. Lysates were then placed on 96-well plates. A PicoGreen assay kit (Invitrogen) was used to measure the absorbance. A BioTek FL800 instrument was used for sample reading at 480/520 nm (ex/em) wavelengths.

Table 1
Sequences of primers used for real-time PCR analysis.

Genes	Sequences
GAPDH	For: 5′-AAC AGC GAC ACC CAC TCC TC
	Rev: 5′-CAT ACC AGG AAA TGA GCT TGA CAA
runx2	For: 5′-AGA TGA TGA CAC TGC CAC CTC TG
	Rev: 5′-GGG ATG AAA TGC TTG GGA ACT
alp	For: 5′-ACC ATT CCC ACG TCT TCA CAT TT
	Rev: 5′-AGA CAT TCT CTC GTT CAC CGC C
opn	For: 5′-ATG AGA TTG GCA GTG ATT
	Rev: 5′-TTC AAT CAG AAA CCT GGA A
oc	For: 5′-TGT GAG CTC AAT CCG GAC TGT
	Rev: 5′-CCG ATA GGC CTC CTG AAG C

DNA concentrations were then determined by comparing values to a standard curve constructed with values for solutions with known DNA concentrations.

To determine alkaline phosphatase activity (ALP), a working solution containing p-nitrophenyl phosphate (p-NPP) was added into samples and then incubated for 30 min at 37 °C. After incubation, the reaction was stopped by placing samples on ice and adding 100 μL of 1 M sodium hydroxide. The absorbance values of samples were obtained on a microplate reader (BioTek) at 405 nm wavelength. The ALP concentration of samples was calculated through a standard curve. The ALP specific activity was determined by normalizing ALP value of each sample to its dsDNA concentration.

2.7. Real-time PCR

Cellular total RNA was extracted after 7 and 14 days of incubation using an RNeasy mini Kit (QIAGEN). RNA concentration was determined on an Eppendorf Biophotometer. RNA samples were then reversed-transcribed into cDNA using an iScript cDNA synthesis kit (BIO-RAD). Real-time PCR was run on an ABI 7900HT Sequence Detection system (ABI, Foster city, CA) using a cDNA product template, specific primers, and iQ SYBR Green supermix (BIO-RAD) in a total volume of 10 μL. Primer sequences as shown in Table 1 for *runx2*, *alp*, osteopontin (*opn*), osteocalcin (*oc*), and glyceraldehyde 3-phosphate dehydrogenase (GAPDH) were purchased from Invitrogen and used to evaluate gene expression [33–35]. The relative genes expression levels were analyzed using the $2^{-\Delta\Delta C_t}$ method [36] by normalizing with the housekeeping gene GAPDH as an endogenous control and calibrating with efficiency, where $\Delta\Delta C_t$ is calculated from $(C_{t,\text{sample}} - C_{t,\text{control}})_{\text{target gene}} - (C_{t,\text{sample}} - C_{t,\text{control}})_{\text{GAPDH}}$.

2.8. Western blot

For Western blot analysis, hMSC were seeded on the β-TCP and ECM/β-TCP scaffolds for 24 h. Cells/scaffolds were then lysed with cold RIPA buffer containing a phosphatase inhibitor cocktail and HaltTM protease (Thermo Scientific, Rockford, IL, USA) for 10 min, and then cell lysates were centrifuged at 15,000 rpm for 15 min at 4 °C to pellet the cell debris. An aliquot of each lysate was taken out to measure protein concentration using a BCA protein assay kit (Thermo Scientific, Rockford, IL, USA). Five μg proteins in a 2× Laemmli loading buffer were heated at 95 °C for 5 min, and separated on 4–15% Mini-Protean TGXTM gels (BIO-RAD). Each lane was loaded with equal protein amounts. A Spectra™ multicolor broad range protein ladder (Fermentas) was run in parallel lanes. After electrophoresis, a PVDF membrane (Millipore, Billerica, MA) was used to transfer the proteins from gels in a buffer (192 mM glycine, 25 mM Tris, and 20% v/v methanol (pH 8.3)) and then washed in 1× TBST washing buffer. The membrane was blocked in 1× TBST with 5% BSA for 1 h at room temperature. Primary antibodies for ERK1/2 and phospho-ERK1/2 (1:1000, Invitrogen) in 1× TBST containing 1% BSA were added onto the PVDF membranes and then incubated overnight at 4 °C. The membranes were rinsed three times in TBST, and the secondary anti-rabbit IgG HRP conjugate (1:2500, Promega) was added and incubated for 1 h at room temperature, followed by another three washes in TBST. The protein bands on the PVDF membrane were visualized in an All-PRO Imaging X-ray film processor (Hicksville, New York) after immersing in ECL Western blotting detection reagents (GE Healthcare, UK) for short time.

2.9. Statistical analysis

In this study all the experimental groups were carried out in triplicate and a Student's *t*-test was used to statistically analyze the difference between groups. Difference was considered significant if the *p* value was less than 0.05.

3. Results

3.1. Characterization of ECM on β-TCP scaffolds

3.1.1. SEM morphologies of ECM

To establish the protocol of producing ECM and the efficacy of decellularization (Fig. 1A), HUVEC were initially seeded on tissue culture plates and decellularized. Light microscopy images of the same field show the morphology of HUVEC after reaching

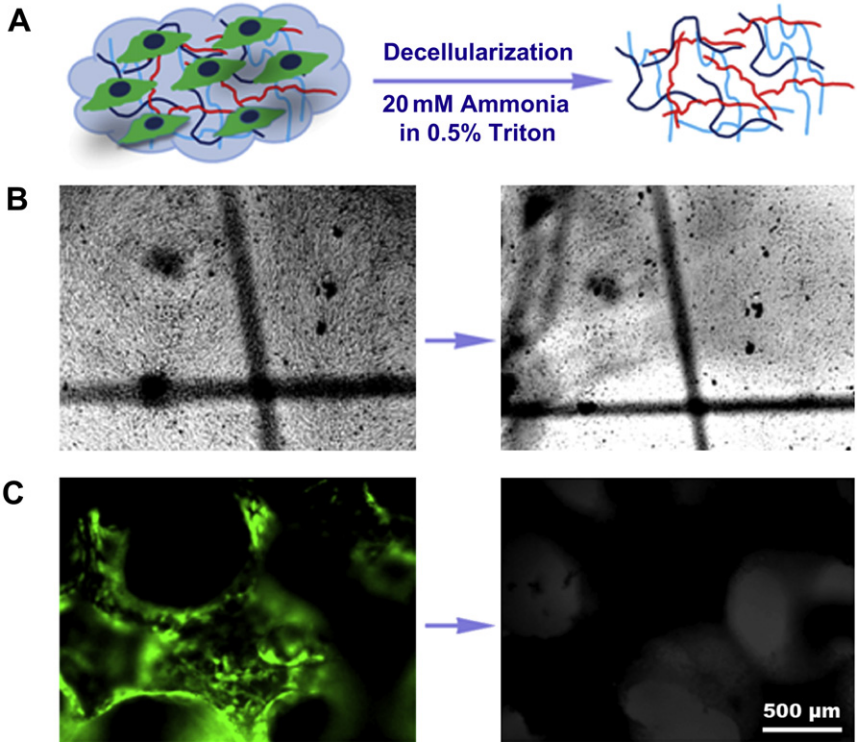

Fig. 1. (A) The schematic of HUVEC-derived ECM production. Left: lines depict ECM, and cells are on the ECM basement; right: ECM after the extraction procedure. (B) Light microscopy images of HUVEC cultured on a tissue culture plate for 14 days after confluence before (left) and after (right) decellularization (right). Location "+" marked identical fields. (C) Fluorescent image of HUVEC cultured on the β-TCP scaffold for 14 days before (left) and after (right) decellularization (magnification: 4×).

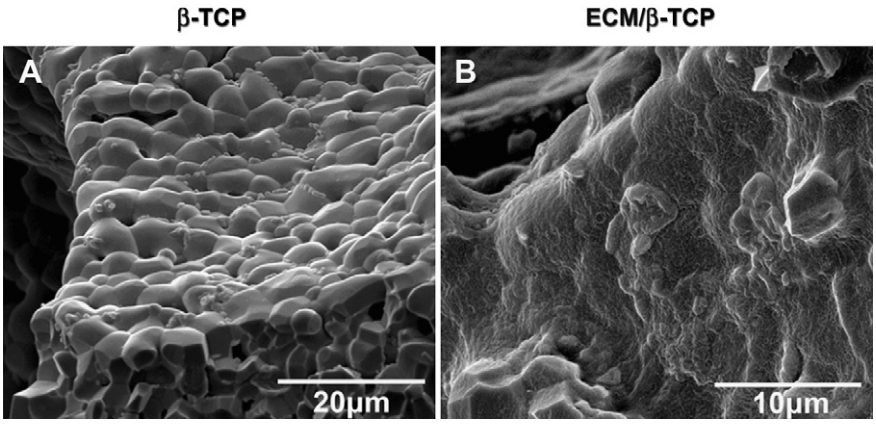

Fig. 2. SEM images of β-TCP scaffold before seeding the HUVEC (left) and of the ECM layer on the β-TCP scaffold after decellularization (right).

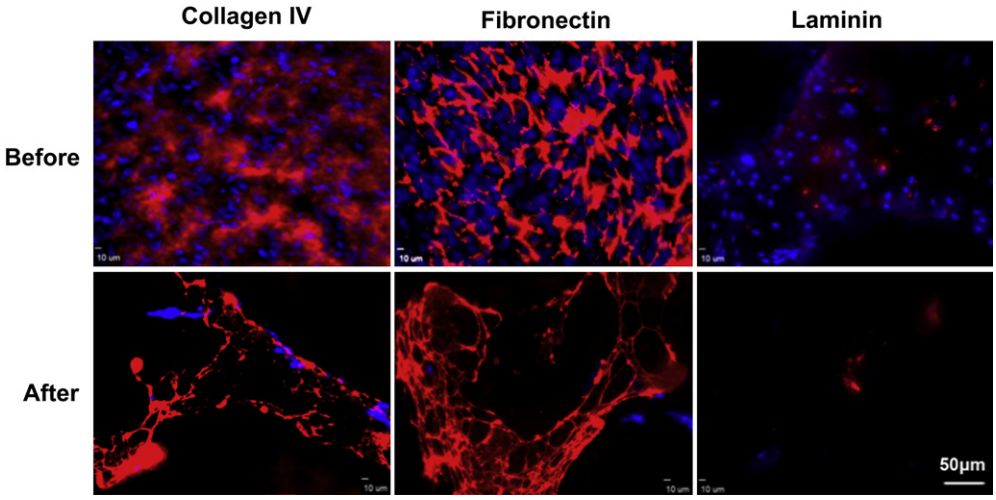

Fig. 3. Immunofluorescent staining images of collagen type IV, fibronectin, and laminin before and after decelluarization. Red: Alexa Fluor® 594 goat anti-mouse antibody; Blue: DAPI. (For interpretation of color in this figure legend, the reader is referred to web version of the article.)

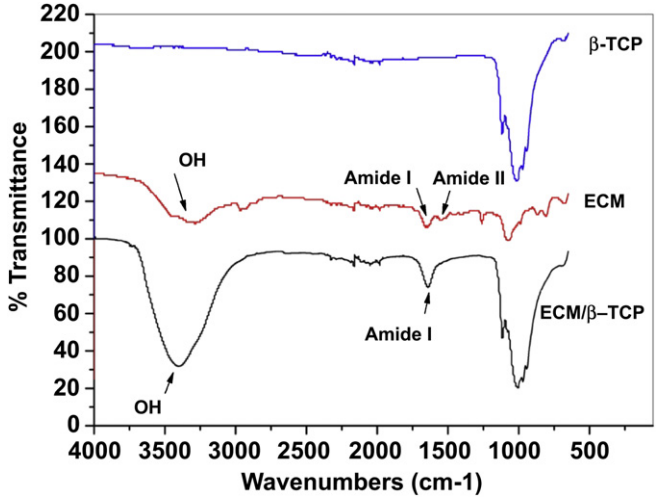

Fig. 4. ATR-FTIR transmission spectra of the β-TCP, ECM from tissue culture plate, and ECM/β-TCP. The characteristic peaks of amide and hydroxyl groups are shown on the ECM and ECM/β-TCP spectrum, respectively.

confluence and the decellularized extracellular matrix (Fig. 1B). Having demonstrated the feasibility of producing decellularized ECM *in vitro*, HUVEC cells/scaffolds were cultured for 14 days on β-TCP scaffolds, and subsequently decellularized. Fig. 1C shows that green GFP-tagged HUVEC cells covered all the surface of the scaffold after culturing for 14 days. No green fluorescence was observed on the scaffold after decellularization. Fig. 2 shows the SEM morphology of the surface of the scaffolds. Surfaces of untreated β-TCP scaffold (β-TCP only) surfaces showed ceramic micrograins and micropores whereas the surfaces of HUVEC ECM-containing β-TCP scaffolds (ECM/β-TCP) contained a dense and heterogeneous coating.

3.1.2. Immunofluorescent staining of collagen IV, laminin and fibronectin

The presence of the ECM on the scaffold was demonstrated using immunofluorescent staining of collagen type IV, laminin, and fibronectin. Results shown in Fig. 3 show that collagen IV and fibronectin produced strong fluorescence intensity, suggesting abundance within the HUVEC ECM, whereas laminin was expressed a relatively low level in a sparse dot-like morphology. After decellularization, the majority of HUVEC were removed, although several nuclei were observed in fluorescent images before and after decellularization. Similarly, these three matrix proteins were present before and after decellularization.

3.1.3. FTIR analysis

Results for FTIR analysis are shown in Fig. 4. The wide bands in the range of 900–1200 cm^{-1} were assigned to characteristic bands of phosphate in β-TCP [37]. These were not observed in the ECM-only spectrum. In the spectra from ECM group, which was harvested from tissue plate after decellularization, two absorption peaks at 1500–1580 cm^{-1} and 1580–1750 cm^{-1} were present and assigned to amide I and amide II. The FTIR spectra of ECM/β-TCP showed two new adsorption bands at 1642.4 cm^{-1} and 3389.3 cm^{-1}, which were absent from the β-TCP only spectrum. As discussed in previous work [38], these peaks corresponded to amide I and hydroxyl groups, respectively. The amide group was assigned to the presence of collagen, while proteoglycans might be responsible for the high hydroxyl group signal [39]. Neither peak was observed in the spectrum of β-TCP only.

3.1.4. XPS analysis

The elements in the ECM/β-TCP scaffolds and the ECM harvested from tissue culture plates were measured by XPS. Result in Fig. 5 showed that there is a new peak (binding energy, 400 eV) in the ECM/β-TCP and ECM-only spectra, corresponding to the amino groups in the peptide bond [32,39]. This peak corresponding to N1s was not observed for ECM-free β-TCP scaffolds. Signal intensity for the C1s peak, at 284.7 eV, was larger for the construct, compared to that of β-TCP only. Table 2 further indicated that the nitrogen atomic percentage in β-TCP only groups was zero, while ECM/β-TCP

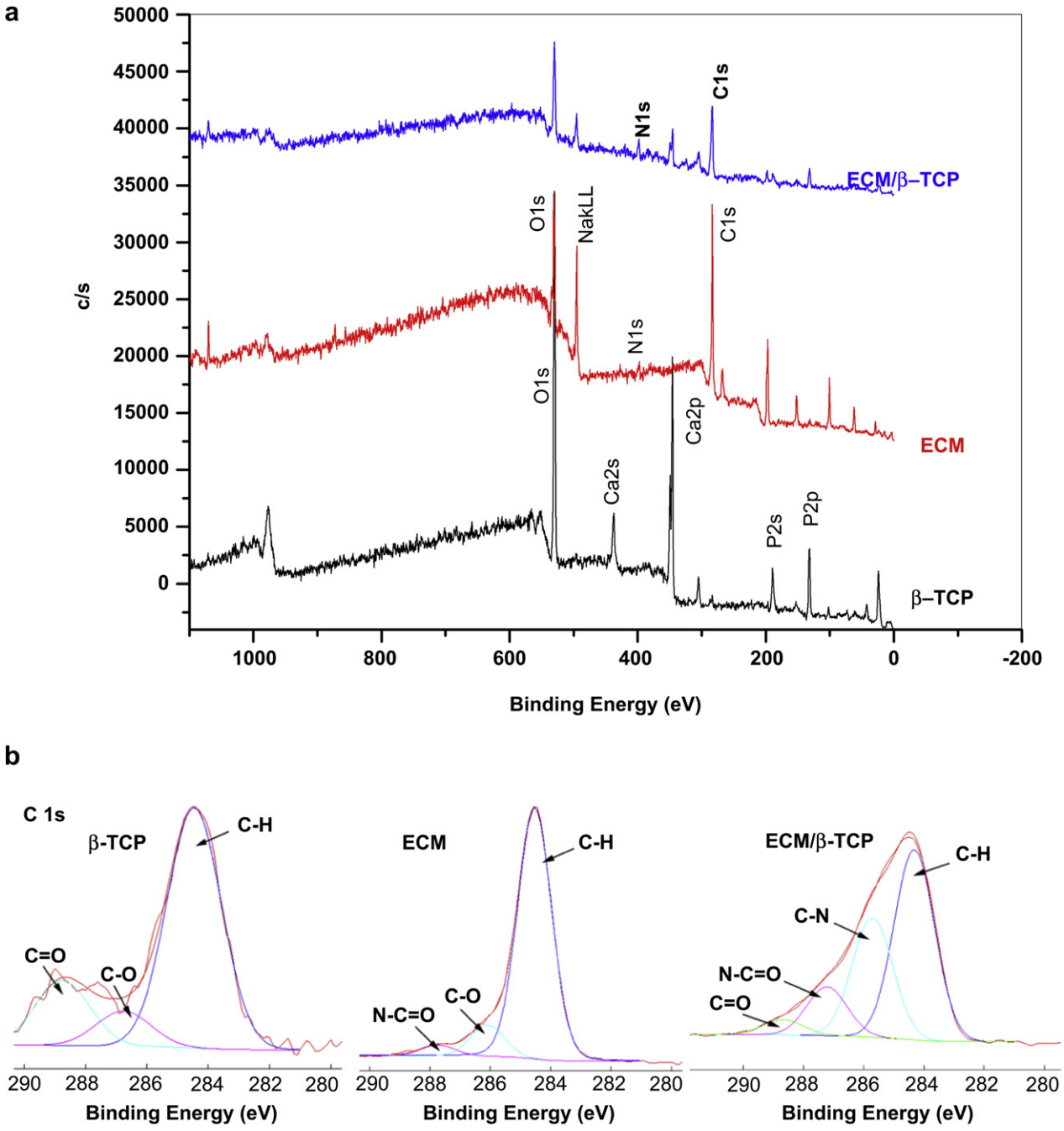

Fig. 5. XPS survey scan spectra (a) and XPS C1s core level spectra (b) for β-TCP, ECM from tissue culture plate, and ECM/β-TCP.

groups contained 1.7%. The carbon atomic percentage in ECM/β-TCP groups was also significantly higher than β-TCP only groups: up to 55.5% in the ECM/β-TCP and 5% in the β-TCP. Trace amounts of carbon in the β-TCP only group were probably attributed to chemical reagents containing carbon during sample processing or from measurement environment. The C1s spectra of β-TCP only, ECM decellularized from tissue culture plates, and ECM/β-TCP groups are demonstrated in Fig. 5b–d, respectively. For the β-TCP only groups, two minor components (286.5 eV (C–O) and 288.8 eV (C=O)) and a main neutral carbon (C–H) component (284.6 eV) were present. For the spectrum of ECM and ECM/β-TCP groups (Fig. 5c, d), two new peaks corresponded to C–N (285.7 eV) and O=C–N (287.6 eV) was shown [39]. These functional groups mainly result from ECM protein biomolecules deposited on the scaffolds.

3.2. Proliferation and osteogenic differentiation of hMSC on β-TCP and ECM/β-TCP scaffolds

3.2.1. dsDNA and ALP

To investigate the effect of ECM on hMSC proliferation and early differentiation, hMSC were seeded on β-TCP only and ECM/β-TCP scaffolds for 3, 7, and 14 days, and the dsDNA content and ALP activity was analyzed. Results in Fig. 6a, b showed no significant difference in dsDNA contents between the β-TCP only and ECM/β-TCP scaffold groups, suggesting that HUVEC-deposited ECM did not alter the proliferation of hMSC. However, the early osteogenic differentiation marker ALP indicates higher activity level in ECM/β-TCP scaffolds than that in β-TCP only scaffolds. This result indicated that ECM deposited on the scaffolds significantly promotes the early differentiation of hMSC.

3.2.2. Real-time PCR

hMSC were seeded on β-TCP only scaffolds and ECM/β-TCP scaffolds for 7 and 14 days, and real-time PCR was performed to analyze the osteogenic gene expression. The results indicated that hMSC cultured in ECM/β-TCP scaffolds showed significantly higher gene expression level of osteogenic transcription factor (*runx2*), early differentiation gene *alp*, and bone extracellular matrix proteins (*opn* and *oc*) after 7 and 14 days, compared to the β-TCP scaffolds (Fig. 7). For *runx2*, hMSC cultured in ECM/β-TCP scaffolds were expressed 5.2-fold higher than that in β-TCP scaffolds after 7 days and 38-fold after 14 days. For *alp*, it was expressed 4.7 and 2.2-fold at 7 and 14 days, respectively. Similarly, *opn* and *oc* genes were also expressed higher fold in ECM/β-TCP scaffolds group than that in β-TCP only scaffolds. Together, these gene expression results demonstrate that HUVEC-derived ECM-containing β-TCP scaffolds significantly up-regulated the expression of osteogenic-related genes.

3.2.3. Immunofluorescence staining of osteocalcin matrix protein

To further verify the significant role of ECM in promoting the osteogenic potential of hMSC, a late-stage extracellular matrix protein of hMSC (osteocalcin) was immunostained. Confocal images showed that the fluorescent density is significantly higher in ECM/β-TCP groups than in the β-TCP only group after culturing for 14 and 21 days (Fig. 8). In β-TCP only group, osteocalcin was sparsely distributed on the scaffold, while it was homogenously dispersed on the ECM/β-TCP scaffold at a high-density. These immunofluorescence results demonstrate that HUVEC-derived ECM-containing β-TCP scaffolds increased deposition of osteogenic ECM in hMSC.

Table 2
The atomic percent of individual elements on the surface of the scaffolds automatically calculated by the software Multipak associated with the equipment.

Groups	Ca2p	P2p	O1s	C1s	N1s	Na1s	Cl2p
β-TCP	18.4	14.3	52.2	5	0	0	0
ECM	0	0	23.2	68.7	5.4	<0.1	2.7
ECM/β-TCP	3.4	7.1	30.8	55.5	1.7	1.2	0.8

3.3. Osteogenic induction of hMSC via MAPK/ERK pathway

To study whether ECM has an effect on the osteogenic differentiation of hMSC through the MAPK/ERK signaling pathway, a inhibitor of the MAPK/ERK signaling pathway, PD98059, was used and its effects on hMSC differentiation were investigated by measuring ALP activity, osteogenic gene expression, and phosphorylated ERK1/2 levels. ALP activity measurements indicated that the inhibitor did not significantly inhibit the ALP activity of hMSC when seeded on β-TCP only scaffolds, whereas ALP activity level of hMSC when seeded on ECM/β-TCP scaffolds was (Fig. 9). Gene expression results indicate that PD98059 inhibitor significantly reduced the expression level of genes *runx2*, *alp*, and *opn*

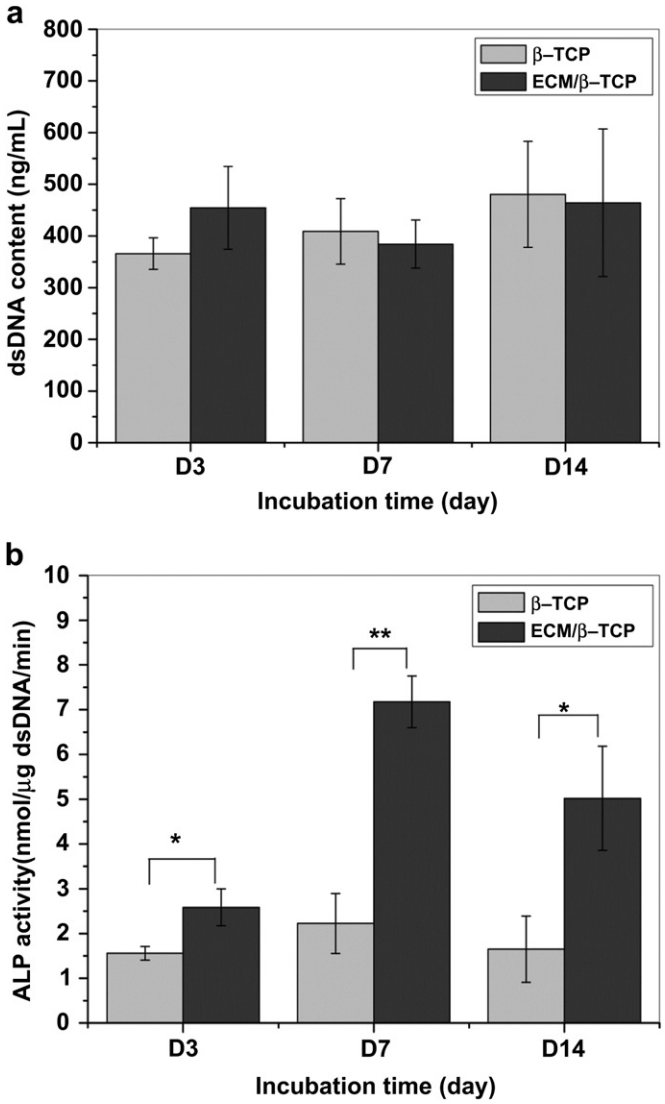

Fig. 6. The amount of dsDNA content synthesized by hMSC grown over time on β-TCP and ECM/β-TCP scaffolds (a). ALP activity of the hMSC on β-TCP and ECM/β-TCP scaffolds (b) ($n = 3$). An * and ** are marked to show significant differences between groups ($^{*}p < 0.05$, $^{**}p < 0.01$).

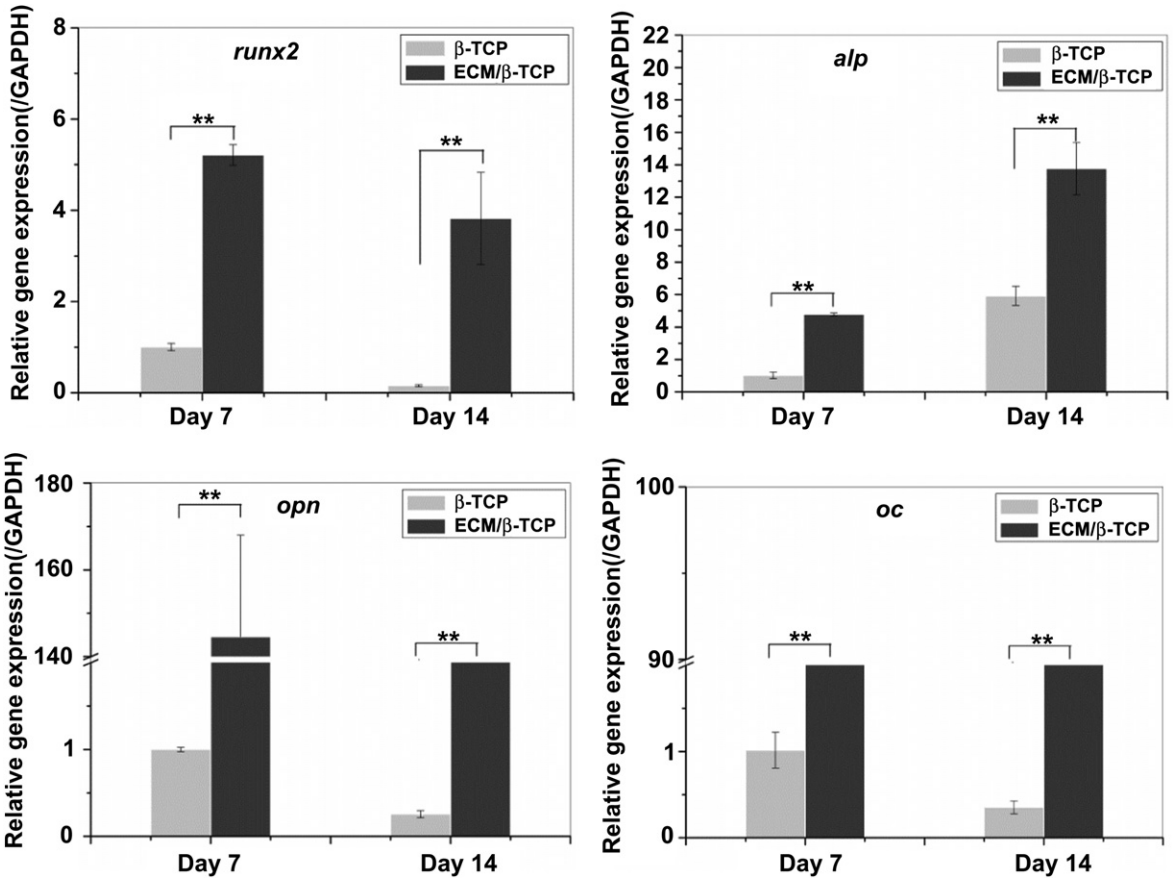

Fig. 7. Related osteogenic gene expression levels in hMSC cultured on β-TCP and ECM/β-TCP scaffolds. *Runx2*, *alp*, *opn* and *oc* gene expression levels were assessed by real-time PCR at days 7 and 14. GAPDH expression was also determined as an internal control. Significant difference between the two groups are shown as * and ** (*$p < 0.05$, **$p < 0.01$).

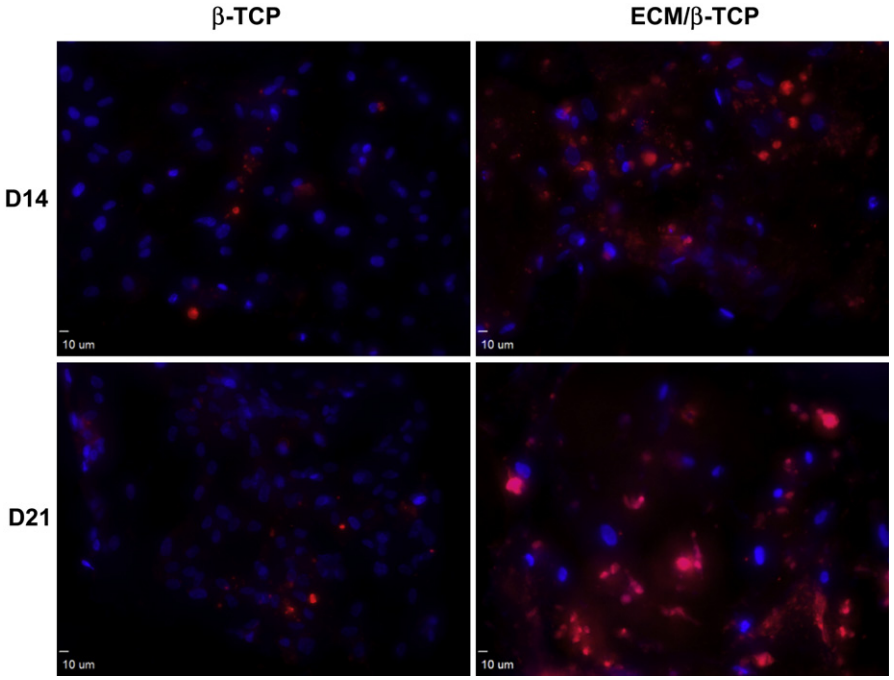

Fig. 8. Confocal microscope images of osteocalcin in hMSC cultured on β-TCP and ECM/β-TCP scaffolds for 14 and 21 days. Red: Alexa Fluor® 594 goat anti-mouse; Blue: DAPI. [For interpretation of color in this figure legend, the reader is referred to web version of the article.]

when hMSC were seeded on ECM/β-TCP scaffold at 7 and 14 days, while it did not inhibit the gene expression of hMSC on β-TCP scaffolds (Fig. 10 for *runx2*, *alp*, *opn*). In addition, Western blot analysis indicated that PD98059 inhibited the expression of phosphorylated protein ERK1/2 24 h after treatment (Fig. 11). Together, these results suggest that ECM increased osteogenic differentiation in hMSC via MAPK/ERK signaling.

4. Discussion

A microenvironment with appropriate spatial and temporal signals will promote tissue regeneration. Porous β-TCP ceramic scaffolds have been developed to provide structural support in bone regeneration; however, these scaffolds lack bioactive components on the surface. ECM can serve as a source of growth factors, cytokines, chemokines and other biological signals, providing bioactive cues for cell proliferation and differentiation. As such, deposition of cell-derived ECM on a 3D porous β-TCP ceramic scaffold potentially creates a biomimetic microenvironment that promotes cellular development by combining biological cues and structural support.

In our previous study, we produced hMSC-derived ECM deposited on CaP scaffolds [27]. In this study, we grew HUVEC on 3D porous β-TCP ceramic scaffolds and then decellularized the construct to generate HUVEC-derived ECM. This was followed by characterization using SEM, FTIR, XPS and immunochemistry. The results demonstrated the presence of ECM components on the surface of CaP scaffolds. It has been reported that endothelial derived ECM is enriched in proteoglycans laminin, collagen IV, and fibronectin. Fibronectin, collagen IV and laminin are thought to be important ECM protein components for cell adhesion, proliferation and differentiation [15,31,32,40–42]. We further used these proteins as biomarkers for the presence of ECM. Our immunofluorescent staining experiments have shown the presence of collagen IV, fibronectin, and laminin on the β-TCP scaffolds.

After the characterization of ECM on the ceramic scaffold, we evaluated whether this HUVEC-derived ECM microenvironment of ECM/β-TCP composite scaffold can promote the osteogenic differentiation of hMSC *in vitro*. We seeded hMSC on the ECM/β-TCP and β-TCP only scaffolds. dsDNA content and ALP activity were measured to determine the extent of cell proliferation and differentiation while the expression of osteogenic genes was determined using real-time PCR. Our study did not demonstrate a significant difference between the ECM/β-TCP and β-TCP scaffold groups in dsDNA content, which provides an indirect measure of cell proliferation. Therefore, the presence of ECM on the scaffold did not significantly promote cell proliferation compared to the plain scaffold condition with incubation time. This may be because we used osteogenic medium, which promotes cells to differentiate but not to proliferate.

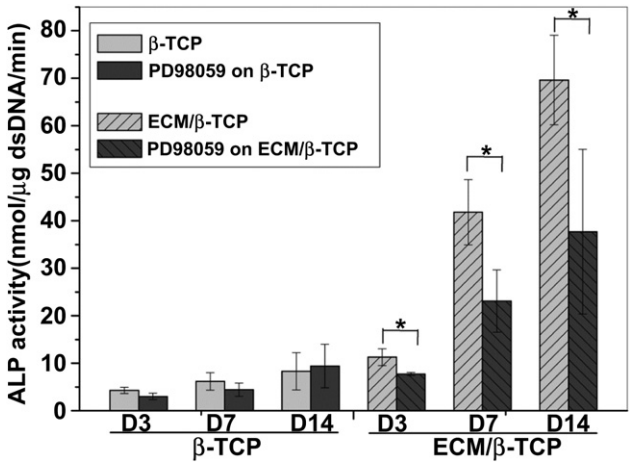

Fig. 9. ALP activity of the hMSC on β-TCP and ECM/β-TCP scaffolds before and after the addition of inhibitor PD98059.

Our results do suggest that ECM plays a significant role in cell differentiation. ALP activity expression levels in ECM/β-TCP scaffolds were significantly higher than those in β-TCP only scaffolds. Bone-related genes were up-regulated in ECM/β-TCP groups compared to β-TCP only groups. The immunofluorescent staining for osteocalcin, a component of bone matrix, was shown to occur at a higher density within ECM/β-TCP scaffolds relative to β-TCP only scaffolds. These results imply that HUVEC-derived ECM promotes early osteogenic differentiation of hMSC *in vitro*. This may be attributable to collagen, fibronectin and laminin proteins in HUVEC-derived ECM, which have previously been reported to stimulate osteogenic differentiation [12,13,15]. However, Kaigler et al. reported that ECM derived from human dermal microvascular endothelial cells did not have any effect on hMSC's osteogenic differentiation. In their experiments, they removed endothelial cells using urea from culture plates and immediately seeded hMSC on the remaining ECM [43]. Villars et al. also reported that HUVEC-derived ECM had no effect on the ALP activity of hMSC [44]. They used glycerol solution to remove cell materials and scraped ECM for dialysis, and then dialyzed ECM solution was homogenously coated for seeding hMSC. Our method is distinct in that we seeded HUVEC on scaffolds and decellularized the constructs using 0.5% Triton solution to remove cells and deposit ECM on the scaffolds. Our finding that HUVEC-derived ECM significantly promoted the osteogenic differentiation of hMSC is distinct from previous studies and this difference may be a result of the unique combination of ECM architecture and CaP scaffolds in a 3D spatial structure.

The early differentiation of hMSC may be mediated by the activation of the MAPK/ERK osteogenic signal pathway [12,15,45,46]. HUVEC-derived ECM deposited on the surface of a scaffold provides new bioactive components, which may activate ERK1/2 expression through the MAPK/ERK signaling pathway mediated by integrins on the cell membrane of hMSC. To determine if the ECM activates the osteogenic differentiation of hMSC through the MAPK/ERK signaling pathway, we used the inhibitor PD98059 to block this MAPK/ERK signaling pathway. ALP activity and gene expression results showed that ALP activity was significantly inhibited and the osteogenic genes were significantly down-regulated in ECM/β-TCP group after PD98059 treatment. This inhibition did not occur in β-TCP group. Similarly, protein expression from Western blotting also showed that the phosphorylated ERK1/2 level in ECM/β-TCP group was significantly inhibited while protein expression in the β-TCP group was not. These results implicate the MAPK/ERK signaling pathway in activating hMSC osteogenic differentiation. ECM components activated this signaling pathway via intergrins on the hMSC membrane, thus down-streaming the osteogenic differentiation pathway of hMSC [15,45,46]. This implies that ECM provides important biological cues for the differentiation of hMSC.

This study reinforces our understanding of cell–matrix interaction in ceramic scaffold-based tissue regeneration techniques. A biomimetic microenvironment provides bioactive cues, regulating the osteogenic behaviors of hMSC. Therefore, through the *in vitro* generation of a cell-derived ECM, the cellular function of a ceramic scaffold can be improved without any additional chemical modification or growth factor binding. This technique could also be used to enhance other tissue regeneration scaffolds. We believe that the clinical impact of this technique could be significant, as the treatment of significant bone defects remains and unsolved problem in

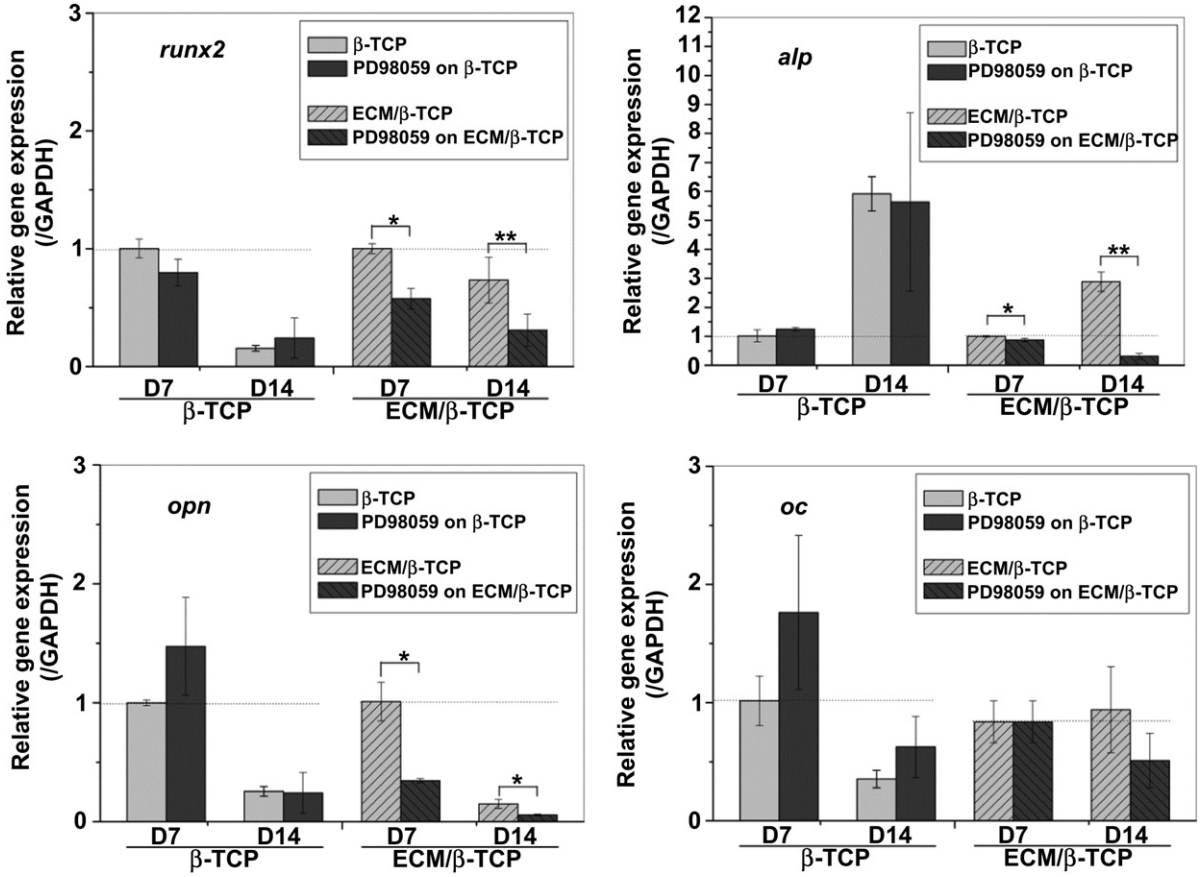

Fig. 10. Related osteogenic gene expression levels in hMSC cultured on ECM/β-TCP scaffolds with and without the presence of inhibitor PD98059. *Runx2*, *alp*, *opn* and *oc* gene expression levels were inhibited by the addition of PD98059. Significant difference between the two groups are shown as * and ** (*$p < 0.05$, **$p < 0.01$).

modern medicine. Our ECM-modified scaffold can be tailored to defects of various shapes and sizes, is easily handled and stored in a clinical setting, and avoids the potential risk of infectious disease.

It is worth noting that in our previous experiments, we seeded hMSC onto 3D porous β-TCP scaffold and generated hMSC-derived ECM-containing porous β-TCP scaffolds [27]. In these studies, we did not observe enhancement of early osteogenic differentiation of hMSC by the hMSC-derived ECM. The difference is that we used an osteogenic medium for the first time in our current study and this combination of HUVEC-derived ECM and osteogenic medium may promote early osteogenic differentiation of hMSC. In the future, we will need to determine if the HUVEC-derived ECM alone will promote early osteogenic differentiation of hMSC in non-osteogenic medium and if the HUVEC-derived ECM will better promote early osteogenic differentiation of hMSC as compared to hMSC-derived ECM in osteogenic medium. Additional research is also indicated to investigate the *in vivo* behaviors of this ECM/scaffold.

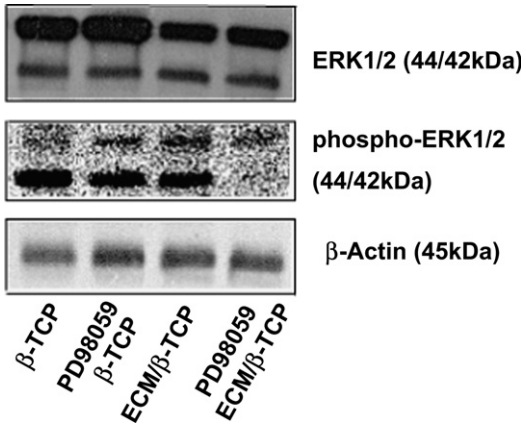

Fig. 11. Protein expression levels of phosphorylated ERK1/2 and total ERK1/2 were evaluated by Western blotting. Blocking MAPK/ERK signaling inhibits the osteogenic differentiation of hMSC on ECM/β-TCP scaffolds. Cell lysates were generated after 24 h. The concentration of total protein was assayed by BCA assay.

5. Conclusion

We fabricated an HUVEC-derived ECM-containing interconnected porous biodegradable β-TCP scaffold. hMSC seeded on this HUEVC ECM-deposited β-TCP scaffold showed increased osteogenic differentiation due to the activation of MAPK/ERK signal pathway. This porous β-TCP with cell-derived ECM provides a promising platform not only for providing mechanical support in a porous structure, but also for mimicing the native cellular microenvironment with biological cues to promote stem cell differentiation.

Acknowledgments

This work was supported by grants from the following agencies: NIH R01AR057837 (NIAMS), NIH R01DE021468 (NIDCR), DOD W81XWH-10-1-0966 (PRORP), W81XWH-10-200-10 (Airlift Research Foundation), W81XWH-11-2-0168-P4 (Alliance of Nano-Health) and Wallace H. Coulter Foundation.

References

[1] Badylak SF, Freytes DO, Gilbert TW. Extracellular matrix as a biological scaffold material: structure and function. Acta Biomater 2009;5:1–13.
[2] Kleinman HK, Luckenbill-Edds L, Cannon FW, Sephel GC. Use of extracellular matrix components for cell culture. Anal Biochem 1987;166:1–13.
[3] Reilly GC, Engler AJ. Intrinsic extracellular matrix properties regulate stem cell differentiation. J Biomech 2010;43:55–62.
[4] Flynn LE, Prestwich GD, Semple JL, Woodhouse KA. Proliferation and differentiation of adipose-derived stem cells on naturally derived scaffolds. Biomaterials 2008;29:1862–71.
[5] Bhrany AD, Beckstead BL, Lang TC, Farwell DG, Giachelli CM, Ratner BD. Development of an esophagus acellular matrix tissue scaffold. Tissue Eng 2006;12:319–30.
[6] Crapo PM, Gilbert TW, Badylak SF. An overview of tissue and whole organ decellularization processes. Biomaterials 2011;32:3233–43.
[7] Badylak S, Liang A, Record R, Tullius R, Hodde J. Endothelial cell adherence to small intestinal submucosa: an acellular bioscaffold. Biomaterials 1999;20:2257–63.
[8] Li WJ, Tuli R, Huang X, Laquerriere P, Tuan RS. Multilineage differentiation of human mesenchymal stem cells in a three-dimensional nanofibrous scaffold. Biomaterials 2005;26:5158–66.
[9] Mauney JR, Kirker-Head C, Abrahamson L, Gronowicz G, Volloch V, Kaplan DL. Matrix-mediated retention of in vitro osteogenic differentiation potential and in vivo bone-forming capacity by human adult bone marrow-derived mesenchymal stem cells during ex vivo expansion. J Biomed Mater Res A 2006;79:464–75.
[10] Mistry AS, Mikos AG. Tissue engineering strategies for bone regeneration. Adv Biochem Eng Biotechnol 2005;94:1–22.
[11] Khademhosseini A, Vacanti JP, Langer R. Progress in tissue engineering. Sci Am 2009;300:64–71.
[12] Kundu AK, Khatiwala CB, Putnam AJ. Extracellular matrix remodeling, integrin expression, and downstream signaling pathways influence the osteogenic differentiation of mesenchymal stem cells on poly(lactide-co-glycolide) substrates. Tissue Eng Part A 2009;15:273–83.
[13] Kundu AK, Putnam AJ. Vitronectin and collagen I differentially regulate osteogenesis in mesenchymal stem cells. Biochem Biophys Res Commun 2006;347:347–57.
[14] Ku Y, Chung C-P, Jang J-H. The effect of the surface modification of titanium using a recombinant fragment of fibronectin and vitronectin on cell behavior. Biomaterials 2005;26:5153–7.
[15] Klees RF, Salasznyk RM, Kingsley K, Williams WA, Boskey A, Plopper GE. Laminin-5 induces osteogenic gene expression in human mesenchymal stem cells through an ERK-dependent pathway. Mol Biol Cell 2005;16:881–90.
[16] Hoshiba T, Lu H, Kawazoe N, Chen G. Decellularized matrices for tissue engineering. Expert Opin Biol Ther 2010;10:1717–28.
[17] Cheng HW, Tsui YK, Cheung KM, Chan D, Chan BP. Decellularization of chondrocyte-encapsulated collagen microspheres: a three-dimensional model to study the effects of acellular matrix on stem cell fate. Tissue Eng Part C Methods 2009;15:697–706.
[18] Choi KH, Choi BH, Park SR, Kim BJ, Min BH. The chondrogenic differentiation of mesenchymal stem cells on an extracellular matrix scaffold derived from porcine chondrocytes. Biomaterials 2010;31:5355–65.
[19] Liao J, Guo X, Grande-Allen KJ, Kasper FK, Mikos AG. Bioactive polymer/extracellular matrix scaffolds fabricated with a flow perfusion bioreactor for cartilage tissue engineering. Biomaterials 2010;31:8911–20.
[20] Wolchok JC, Tresco PA. The isolation of cell derived extracellular matrix constructs using sacrificial open-cell foams. Biomaterials 2010;31:9595–603.
[21] Silva EA, Mooney DJ. Synthetic extracellular matrices for tissue engineering and regeneration. In: Current topics in developmental biology. Academic Press; 2004. p. 181–205.
[22] Pham QP, Kasper FK, Scott Baggett L, Raphael RM, Jansen JA, Mikos AG. The influence of an in vitro generated bone-like extracellular matrix on osteoblastic gene expression of marrow stromal cells. Biomaterials 2008;29:2729–39.
[23] Datta N, Holtorf HL, Sikavitsas VI, Jansen JA, Mikos AG. Effect of bone extracellular matrix synthesized in vitro on the osteoblastic differentiation of marrow stromal cells. Biomaterials 2005;26:971–7.
[24] Datta N, Pham QP, Sharma U, Sikavitsas VI, Jansen JA, Mikos AG. In vitro generated extracellular matrix and fluid shear stress synergistically enhance 3D osteoblastic differentiation. Proc Natl Acad Sci U S A 2006;103:2488–93.
[25] Thibault RA, Scott Baggett L, Mikos AG, Kasper FK. Osteogenic differentiation of mesenchymal stem cells on pregenerated extracellular matrix scaffolds in the absence of osteogenic cell culture supplements. Tissue Eng Part A 2010;16:431–40.
[26] Chen XD, Dusevich V, Feng JQ, Manolagas SC, Jilka RL. Extracellular matrix made by bone marrow cells facilitates expansion of marrow-derived mesenchymal progenitor cells and prevents their differentiation into osteoblasts. J Bone Miner Res 2007;22:1943–56.
[27] Kang Y, Kim S, Khademhosseini A, Yang Y. Creation of bony microenvironment with CaP and cell-derived ECM to enhance human bone-marrow MSC behavior and delivery of BMP-2. Biomaterials 2011;32:6119–30.
[28] Liu Y, Kim JH, Young D, Kim S, Nishimoto SK, Yang Y. Novel template-casting technique for fabricating beta-tricalcium phosphate scaffolds with high interconnectivity and mechanical strength and in vitro cell responses. J Biomed Mater Res A 2010;92:997–1006.
[29] Kang Y, Scully A, Young DA, Kim S, Tsao H, Sen M, et al. Enhanced mechanical performance and biological evaluation of a PLGA coated beta-TCP composite scaffold for load-bearing applications. Eur Polym J 2011;47:1569–77.
[30] Melero-Martin JM, De Obaldia ME, Kang SY, Khan ZA, Yuan L, Oettgen P, et al. Engineering robust and functional vascular networks in vivo with human adult and cord blood-derived progenitor cells. Circ Res 2008;103:194–202.
[31] Matsubara T, Tsutsumi S, Pan H, Hiraoka H, Oda R, Nishimura M, et al. A new technique to expand human mesenchymal stem cells using basement membrane extracellular matrix. Biochem Biophys Res Commun 2004;313:503–8.
[32] Xue X, Wang J, Zhu Y, Tu Q, Huang N. Biocompatibility of pure titanium modified by human endothelial cell-derived extracellular matrix. Appl Surf Sci 2010;256:3866–73.
[33] Yim EK, Wan AC, Le Visage C, Liao IC, Leong KW. Proliferation and differentiation of human mesenchymal stem cell encapsulated in polyelectrolyte complexation fibrous scaffold. Biomaterials 2006;27:6111–22.
[34] Anderson JM, Vines JB, Patterson JL, Chen H, Javed A, Jun HW. Osteogenic differentiation of human mesenchymal stem cells synergistically enhanced by biomimetic peptide amphiphiles combined with conditioned medium. Acta Biomater 2011;7:675–82.
[35] Hofmann A, Ritz U, Verrier S, Eglin D, Alini M, Fuchs S, et al. The effect of human osteoblasts on proliferation and neo-vessel formation of human umbilical vein endothelial cells in a long-term 3D co-culture on polyurethane scaffolds. Biomaterials 2008;29:4217–26.
[36] Livak KJ, Schmittgen TD. Analysis of relative gene expression data using real-time quantitative PCR and the 2−[Delta][Delta]CT method. Methods 2001;25:402–8.
[37] Coelho PG, Coimbra ME, Ribeiro C, Fancio E, Higa O, Suzuki M, et al. Physico/chemical characterization and preliminary human histology assessment of a [beta]-TCP particulate material for bone augmentation. Mater Sci Eng C 2009;29:2085–91.
[38] Yang MC, Wang SS, Chou NK, Chi NH, Huang YY, Chang YL, et al. The cardiomyogenic differentiation of rat mesenchymal stem cells on silk fibroin-polysaccharide cardiac patches in vitro. Biomaterials 2009;30:3757–65.
[39] Wen F, Chang S, Toh YC, Teoh SH, Yu H. Development of poly (lactic-co-glycolic acid)-collagen scaffolds for tissue engineering. Mater Sci Eng C 2007;27:285–92.
[40] Kleinman HK, Philp D, Hoffman MP. Role of the extracellular matrix in morphogenesis. Curr Opin Biotech 2003;14:526–32.
[41] Cagliero E, Roth T, Roy S, Lorenzi M. Characteristics and mechanisms of high-glucose-induced overexpression of basement membrane components in cultured human endothelial cells. Diabetes 1991;40:102–10.
[42] Beltramo E, Pomero F, Allione A, D'Alu F, Ponte E, Porta M. Pericyte adhesion is impaired on extracellular matrix produced by endothelial cells in high hexose concentrations. Diabetologia 2002;45:416–9.
[43] Kaigler D, Krebsbach PH, West ER, Horger K, Huang YC, Mooney DJ. Endothelial cell modulation of bone marrow stromal cell osteogenic potential. FASEB J 2005;19:665–7.
[44] Villars F, Bordenave L, Bareille R, Amedee J. Effect of human endothelial cells on human bone marrow stromal cell phenotype: role of VEGF? J Cell Biochem 2000;79:672–85.
[45] Xiao G, Jiang D, Thomas P, Benson MD, Guan K, Karsenty G, et al. MAPK pathways activate and phosphorylate the osteoblast-specific transcription factor, Cbfa1. J Biol Chem 2000;275:4453–9.
[46] Osyczka AM, Leboy PS. Bone morphogenetic protein regulation of early osteoblast genes in human marrow stromal cells is mediated by extracellular signal-regulated kinase and phosphatidylinositol 3-kinase signaling. Endocrinology 2005;146:3428–37.